Structure and Dynamics of 9(10H)-Acridone and Its Hydrated Clusters. I. Electronic Spectroscopy

Masaaki Mitsui[†] and Yasuhiro Ohshima*

Department of Chemistry, Graduate School of Science, Kyoto University, Kitashirakawa-Oiwakecho, Sakyo-ku, Kyoto 606-8502, Japan

Received: March 20, 2000; In Final Form: July 5, 2000

A series of papers (I−III) reports spectroscopic investigation on structure and dynamics of 9(10H)-acridone (AD) and its hydrated clusters. As the first part of the series, the present paper describes their lowest $^1(\pi,\pi^*)$ electronic transition in the 370−400 nm region studied by fluorescence-based laser spectroscopy and mass-selective two-color resonance-enhanced two-photon ionization (2C-R2PI). Thirteen fluorescent hydrates as well as the monomer have been identified in fluorescence-excitation and UV−UV hole-burning measurements, and size assignments for relatively smaller clusters, AD−$(H_2O)_n$ (n = 1−6), have been conducted by 2C-R2PI. The origin bands for larger-size clusters show larger red shifts converging at ca. 2200 cm^{-1} but the changes are nonmonotonic, with a substantial increase from n = 2 to 3. Density-functional-theory (DFT) calculations at the B3LYP/6-31G(d,p) level have predicted that the energy difference between the C═O and N−H bonded isomers is quite small (only ≈ 1 kcal/mol) for n = 1 and 2. The observed spectral shifts of fluorescent hydrates with n = 1 and 2 are well reproduced by the HOMO−LUMO gap in the DFT orbital energies of either of the N−H or C═O bonded isomers, leaving the definitive structural assignments to fluorescence-detected infrared spectroscopy which will be described in paper II. For the larger clusters (n = 3−5), several minimum-energy structures have been identified within 2 kcal/mol in binding energy, among which the conformers with water molecules bridging between the C═O and N−H sites over the AD's aromatic rings are identified as the observed species, based on good agreement between the calculated and observed spectral shifts.

1. Introduction

It has been well realized that static and dynamical properties of molecules can be considerably influenced by local environments surrounding them.[1,2] For instance, some aromatic dyes show pronounced sensitivity in fluorescence (i.e., absorbing and emitting wavelength, fluorescence lifetime, etc.) to solvents, so they serve as a useful probe for local conditions in inhomogeneous media, e.g., micelles, membranes, micropores, and biological systems.[2] Understanding of such microscopic "solvation" effects requires molecular-level description of short-range intermolecular interactions, which should be much different for each interacting site in a molecule. These site-specific interactions perturb the electron distribution in the molecule so strongly that the resultant large shifts in electronic states cause drastic changes in photochemical and/or photophysical behaviors. In addition, detailed knowledge on perturbation in a solute by nearby solvent molecule(s) is indispensable for supporting and extending theoretical models developed so far to describe solvation effects in condensed media.

Molecular clusters have been regarded as useful model systems to examine some of the interactions responsible for the solvation effects on a molecular scale, since we can probe a stepwise evolution of molecular properties by successively increasing the number of solvent molecules. Systematic investigation on dynamics of solute molecules with well-defined solute-$(solvent)_n$ geometry has been thus one of the most attractive subjects on clusters. Some previous studies have already addressed partial appreciation of these dynamics. Dynamical behaviors in clusters of phenol[3−5] and 1-naphthol[6−8] solvated with ammonia are pedantic examples of distinct cluster-size dependence on chemical reactions (excited-state proton-transfer in this case). $(Naphthalene)_n$ have indicated an irregular change in excimer formation rates in respect to cluster size, which has been explained as a conformation-controlled phenomenon.[9] Charge-transfer reaction in 9,9′-bianthryl solvated with polar molecules has been reported to depend sharply on symmetric or asymmetric solvation.[10] Remarkable site-specific changes in electronic-excitation and ionization energies have also been identified in hydrated clusters of a coumarin dye.[11] As most closely related to the present study, notable changes in fluorescence lifetimes by microscopic solvation have been identified for isoquinoline clusters with several polar solvents.[12]

All the above-mentioned studies have demonstrated strong correlation of solute dynamics to microscopic solvation, yet conclusive discussions on geometry of the clusters thus examined still remain for further study. This is mainly because of the difficulty in structural characterization of clusters with various sizes, but the situation has been improved substantially in the past few years. On the experimental side, developments of double resonance techniques with infrared (IR) or stimulated-Raman excitation[13,14] have made the largest contribution. These highly sensitive methods provide vibrational spectra of clusters with relatively larger sizes in a species-selected manner. Vibrational spectra thus obtained for hydrogen-bonded clusters

* Corresponding author. Fax: +81-75-753-3974. E-mail: ohshima@kuchem.kyoto-u.ac.jp.

[†] Research Fellow of the Japan Society for the Promotion of Science for Young Scientists, 1997−1999.

10.1021/jp001047+ CCC: $19.00
Published on Web 08/31/2000

are quite useful to address their bonding topologies, because frequency shifts in hydride stretching vibrations are quite sensitive to the site-specific H bonding. Along with the experimental advances, acceptably accurate molecular-orbital calculations become available even for relatively larger systems owing to the improvements in ab initio and density-functional-theory (DFT) algorithms as well as rapid progress in computational capability. Comparison with experimental results can afford unequivocal characterization of H-bonding networks, as has been shown in studies of various H-bonded aromatic clusters.[15−18]

Among various photochemical and photophysical reactions, nonradiative processes mediated by internal conversion (IC) and intersystem crossing (ISC) are of the best to be explored. First, IC and ISC are general energy-dissipation pathways, which frequently lead to various subsequent reactions.[19] Second, their reaction mechanisms have been extensively studied in condensed phase and under supersonic-jet conditions.[20] Electronic states involved in the relaxation processes are relatively well characterized, and many dynamical aspects have been established as mentioned below. Third, there are many molecules, aromatic carbonyls and *N*-heterocyclic compounds in most cases, which show pronounced solvation effects on the nonradiative processes in liquid solution.[21−28] Generally, fluorescence intensities of the molecules are extremely weak in nonpolar solvents but become moderately strong in H-bonding solvents such as water. It implies that site-specific interactions should play an important role in controlling the dynamics, and this issue can be addressed in much detail by using clusters solvated with H-bonding molecules, for which solvation structure can be most thoroughly characterized via combination of IR-spectroscopic and computational methods.

It is well known that IC and/or ISC operative in aromatic carbonyls and *N*-heterocyclic compounds are often related to the energetics of two electronic states with different configurations, i.e., (π,π^*) and (n,π^*). If the (π,π^*) and (n,π^*) states with the same multiplicity are located close each other in excitation energy, the vibronic coupling between the two nearly degenerate states through out-of-plane bending mode(s) strongly enhances the IC from these states to lower electronic state(s) (so-called proximity effect).[21,29] The (π,π^*) $\leftrightarrow$ (n,π^*) type interaction for singlet $\leftrightarrow$ triplet ISC is also strong due to large spin−orbit coupling matrix elements between them (El-Sayed's rules).[19,22] Therefore, the close spacing between the (π,π^*) and (n,π^*) states facilitates the fast nonradiative decay process(es). This situation holds for the molecules exhibiting pronounced solvation effects on fluorescence, if they are in nonpolar solvents.[24,27] In the case of H-bonding solvents, the energy spacing becomes substantially larger since the (n,π^*) state is generally shifted to higher energy via H-bonding interaction, whereas the (π,π^*) state is slightly red-shifted. Hence, the nonradiative processes are considerably suppressed in this class of solvents.[21−28]

On the basis of the above-mentioned background, we have started studies on solvated clusters of aromatic molecules displaying prominent solvation effects, with the aim at clarifying the interplay between solvent geometry, vibronic-energy structure, and nonradiative dynamics. Aromatic carbonyl and *N*-heterocyclic molecules chosen for our study are 9(10H)-acridone and acridine, respectively. As regards acridine, we have recently reported vibrational spectroscopy of its hydrated clusters containing up to three water molecules,[30] and further discussion on the nonradiative dynamics will be given in a forthcoming paper.[31] In this series of the papers (I−III), we represent full accounts on experimental and computational results obtained for 9(10H)-acridone (hereafter abbreviated as AD) and its hydrated clusters. This molecule is chosen as a model system

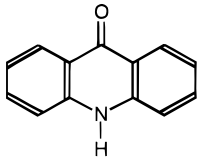

among aromatic carbonyl compounds for several reasons. First, remarkable solvation effects (H-bonding effects) on nonradiative processes in AD have been identified in liquid solution.[23,32−34] Accumulated knowledge of its electronic-energy levels and fluorescence properties in various solvents should be valuable for detailed comparison with results of the clusters. Second, AD is a planar rigid molecule with C_{2v} symmetry.[35] Owing to the rigidity of the system, any experimentally measured kinetics can be assigned to photophysical processes, and not to significant changes of structure in the excited state or photochemical processes. Last, AD has multiple H-bonding sites, i.e., C═O, N−H, and π-aromatic rings, thus it is particularly suitable for investigating site-specificity in solvation (H-bonding) effects on nonradiative dynamics.

This series of papers (I−III) is outlined as follows. Paper I represents electronic spectroscopy for fluorescent hydrated AD clusters via fluorescence-excitation, UV−UV hole-burning, and two-color resonance-enhanced two-photon ionization methods. DFT computational results on optimized geometry, binding energy, and spectral shift in electronic transition are also described. H-bonding topologies in the clusters are discussed by comparing the observed and calculated spectral shifts in the electronic transitions. Paper II describes the results from fluorescence-detected infrared (FDIR) spectroscopy and their analyses via DFT calculations. We provide firm structural assignments for experimentally observed clusters, and also discuss characteristic solvation structure and its evolution with increasing degrees of hydration. Paper III presents the results from frequency- and time-domain experiments on nonradiative dynamics of AD and its hydrated clusters. On the basis of cluster geometry obtained in the first two papers, we discuss the molecular-scale correlation of their dynamics to size-specific and site-specific H-bonding nature in the hydrates.

2. Experimental and Computational Procedures

2.1. Fluorescence-Excitation and UV−UV Hole-Burning Spectroscopy. Details of the experimental setup for the fluorescence-excitation (FE) measurement have been presented elsewhere.[30] UV−UV hole-burning (HB) measurements employed two laser pulses in the similar wavelength region (365−400 nm in this case), which were temporally separated from each other by $\approx$ 200 ns. The first laser (denoted as *burn*) was scanned across the vibronic bands observed in the FE spectrum, while the second laser (denoted as *probe*) was fixed to the electronic origin of the species being studied. Depletion in the ground-state population by the burn pulse was monitored as decrease in fluorescence by the probe pulse. To induce the population hole as large as possible, strong burn pulses (up to several mJ/pulse) were delivered from a XeCl excimer-laser pumped dye laser (Lambda-Physik LPX100/LPD3000 with DMQ, BBD, BBQ, or PBBO dye), while the doubled output (well below 0.1 mJ/pulse) of a dye laser (LAS, LDL205 with LDS 751 or 798) pumped by a Nd^+:YAG laser (Spectra Physics, GCR-4) was used as the probe.

Hydrated clusters of acridone were generated in a supersonic expansion from a pulsed solenoid valve (General Valve, Series 9) with a 0.8-mm-diameter orifice. The solid sample was placed in a small holder, which was directly attached to the valve. The sample holder and the valve were heated (190−200 °C) by a sheath heater surrounding them. The sample vapors were entrained in helium carrier gas at a stagnation pressure of 2−4 atm, and pulsed out into the chamber at 10 Hz repetition rate. Water vapor was incorporated into the carrier gas by adding moisturized helium gas, which passed through a water vessel held at room temperature. Concentration of water was adjusted by changing the mixing ratio with a needle valve.

2.2. Resonance-Enhanced Two-Photon Ionization Mass Spectrometry. Mass-selective experiments described in this work have been performed with a recently constructed time-of-flight mass spectrometer (TOF-MS). The apparatus consists of three differentially pumped regions for molecular-beam source, ionization, and TOF mass analysis. The source chamber is evacuated by an 8 in. diffusion pump backed by a root blower pump and a rotary pump in series. The ionization chamber is evacuated by an 6 in. diffusion pump with a liquid nitrogen-cooled trap backed by a rotary pump. The TOF tube is evacuated by a 250 L/s turbo molecular pump backed by a rotary pump. The pumping system produces base pressures of better than 10^{-6}, 10^{-6}, and 10^{-7} Torr in the source, ionization, and TOF regions, respectively. The apparatus is equipped with a linear reflectron-type TOF-MS unit (R. M. Jordan, LRMS), which has been used in Wiley−McLaren configuration[36] throughout in this study. Molecular beams from a pulsed solenoid valve (General Valve, Series 9) with a 0.8-mm orifice were collimated by a conical skimmer (Beam Dynamics, 1.0 mm orifice) located 3−5 cm from the valve. After 20 cm travel from the skimmer, the beams are photoionized between a pair of electrodes. The resultant ions are perpendicularly accelerated by a DC electric field into the 72-cm-long flight region and detected by a dual-assembly microchannel plate (MCP) detector (Gallileo). Mass resolution of the TOF-MS system is $M/\Delta M \approx 420$ at $M = 500$. The output from the MCP was preamplified and averaged by a digital oscilloscope (LecLoy, 9310AM) to obtain mass spectra. To record mass-selective excitation spectra, the signal was averaged by a boxcar integrator (SRS, SR250), digitized by an A/D converter, and finally stored into a personal computer for further data processing.

The vertical ionization energy (IE_v) of acridone, which has been determined to be 7.69 eV ($\approx$ 62000 cm^{-1}) by a HeI photoelectron experiment,[37] is higher than twice of the $S_1 \leftarrow S_0$ electronic excitation, identified as 27265 cm^{-1} by the present FE measurement. Therefore, two-color resonance-enhanced two-photon ionization (2C-R2PI) has been adopted for mass assignments of hydrated AD clusters. The present 2C-R2PI measurements employed two independent dye lasers. The doubled output of the first dye laser (LAS, LDL205 with LDS 751 or 798) pumped by a Q-switched Nd^+:YAG laser (Spectra Physics, GCR-4) served as the $S_1 \leftarrow S_0$ excitation source (λ_{res}) and was tunable in the 360−400 nm region. The second dye laser (Continuum, ND6000 with Coumarin 3 or 153), pumped by the third harmonic of another Nd^+:YAG laser (Continuum, Surelite II-10), was also frequency-doubled to generate the ionization photon (λ_{ion}) between 250 and 290 nm. Autotracking units (Inrad, AT-III) with a KDP or BBO crystal were used for second-harmonic generation of the dye laser outputs. It is noted that the ground-state AD does not strongly absorb the λ_{ion} photon in this region, so the one-color background signal due to the two-photon excitation by λ_{ion} can be easily controlled by changing the ionization laser power. The firings of both lasers were triggered by a digital delay/pulse generator (SRS, DG535), and the delay for λ_{ion} relative to λ_{res} was fixed at 1−10 ns. Two unfocused dye laser beams with $\approx$3 mm diameters were counterpropagated and directed into the interaction region of the linear TOF-MS at a right angle to the molecular beam axis. Gas sample handling was the same as described above, with exception of slightly higher stagnation pressure (3−8 atm). Pressures in the chambers were maintained at $\approx 10^{-4}$, 10^{-6}, and 10^{-7} Torr in the source, ionization, and TOF regions, respectively, during the measurements.

2.3. Molecular Orbital Calculations. Ab initio and density-functional-theory (DFT) molecular-orbital calculations of AD and its hydrated clusters have been carried out with a suite of Gaussian 98 programs[38] as follows.

As extensive surveys for possible geometries, minimum-energy structures of $AD-(H_2O)_n$ ($n = 1-5$) were searched for at the RHF/6-31G level with various initial configurations for solvents. All geometrical optimizations have been conducted without any symmetry constraint. The initial geometry of the solute in the clusters was set to the optimized structure for bare AD, which was a C_{2v} planar structure. The AD molecule has two hydrogen-bonding sites, i.e., the carbonyl group, which acts as an H accepting site, and the N−H group as an H donor. The π clouds of the AD aromatic rings may also act as an H acceptor, even though π-H bonding should be much weaker than those to the former two sites. Solvent units were thus put so as to interact with each (or two) of the three sites in the initial configurations. Both chain- and cyclic-type $(H_2O)_n$ were considered as binding units for $n \geq 3$. For $n = 2-5$, in addition, "separately bonded" type clusters with two solvent units independently bound to the C═O and N−H sites have been examined.

The stable structures thus identified by the global surveys were further optimized by DFT calculations using the Becke3LYP functional[39,40] with a 6-31G(d,p) basis set. Force fields were calculated for such optimized structures to ensure that they represented true potential minima. Harmonic frequencies and infrared intensities for all vibrational modes were calculated to be compared with observed spectra (as described in paper II) and to obtain zero-point vibrational energy (ZPVE) corrections. The total binding energies, $-\Delta E_0^B$ and $-\Delta E_0^N$, required for $AD-(H_2O)_n$ to dissociate into AD + nH_2O, were calculated with and without basis set superposition error (BSSE) corrections, respectively. The standard counterpoise procedure[41] was utilized to obtain the binding energies with BSSE corrections. HOMO and LUMO orbital energies thus evaluated for the optimized structures were used to estimate the spectral shifts in the electronic transition of the hydrated clusters.

3. Experimental Results

3.1. FE and UV−UV HB Spectra of AD and Its Hydrated Clusters. An overview of the FE spectrum is presented in Figure 1. A number of bands are spread over in a wavelength region covering more than 30 nm. All of the observed bands except for a very weak one denoted as "A" became stronger when the water vapor was introduced into the carrier gas. This observation indicates that band A is that of the monomer while all the others are due to hydrated clusters of AD. When the experimental conditions were changed, intensities changed from band to band, implying that many different clusters have contributed to the observed FE spectrum. The bands showing larger red shifts seemed to be due to clusters with larger sizes, since they appeared at higher water concentration and higher stagnation pressure.

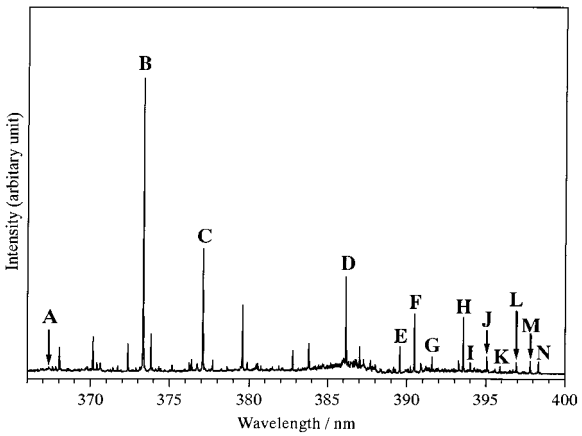

Figure 1. Fluorescence-excitation (FE) spectrum of AD−$(H_2O)_n$ under jet-cooled conditions. The 366−387 and 387−400 nm regions of the FE spectrum have been recorded under the stagnation pressure of 2.0 and 3.5 atm, respectively. A is the origin band of the $^1(\pi,\pi^*)$ electronic transition for bare AD and B−N are those of hydrated AD clusters.

TABLE 1: Transition Frequencies of the $^1(\pi,\pi^*)$ Electronic Origins and the Spectral Shifts of Acridone−$(H_2O)_n$ (cm^{-1})

species[a]	$^1(\pi,\pi^*)$ electronic origin	spectral shift[b]
A (AD monomer)	27265	0
B ($n = 1$)	26793	−472
C ($n = 2$)	26525	−740
D ($n = 3$)	25901	−1364
E ($n = 4$)	25676	−1589
F ($n = 5$)	25616	−1649
G	25433	−1832
H ($n = 6$)	25414	−1851
I	25396	−1869
J	25318	−1947
K	25264	−2001
L	25199	−2066
M	25142	−2123
N	25110	−2155

[a] Mass assignments were made by 2C-R2PI measurements. [b] Relative to the origin of the AD monomer.

To clarify how many species are present in the observed FE spectrum, we have performed the UV−UV HB measurements. The resultant HB spectra have revealed the presence of 13 different hydrated clusters, and the bands denoted as B−N have been assigned to their origin bands of the $^1(\pi,\pi^*)$ electronic transition. All other peaks in the FE spectrum have been identified as vibronic transitions of the 13 species, i.e., B−N. Transition frequencies of the $^1(\pi,\pi^*)$ electronic origins of A−N are summarized in Table 1. Mass assignments have been further conducted for smaller clusters, as described in the next section.

Spectral shifts in the $^1(\pi,\pi^*)$ electronic transition of the hydrated clusters are to be mentioned in some detail. Species B ($n = 1$) shows relatively large red shift (472 cm^{-1}), and the increment to species C ($n = 2$) becomes almost half of it (268 cm^{-1}). However, the next larger cluster (species D, $n = 3$) shows a much larger incremental red shift (624 cm^{-1}), and the increments to $n = 4$ and 5 (species E and F, respectively) are much reduced again (225 and 60 cm^{-1}). This characteristic change in the spectral shifts will be discussed in section 5 of this paper. All of the origin bands of larger clusters (species G−N) fall within a narrow region (red-shifted by 1800−2200 cm^{-1}), and the intervals between successive bands are well below 100 cm^{-1}. Thus the red shifts seem to be gradually saturated as the cluster sizes become larger, though precise increments cannot be determined because of the luck of their mass assignments. It has been reported that AD in an H-bonded solvent, e.g., ethanol, has an absorption maximum at ca. 410 nm (red-shifted by ≈ 3000 cm^{-1} from bare AD).[42] The red shifts for the hydrated clusters with $n \approx 10$ (species L, M, and N) have already reached to more than two-thirds of the bulk value.

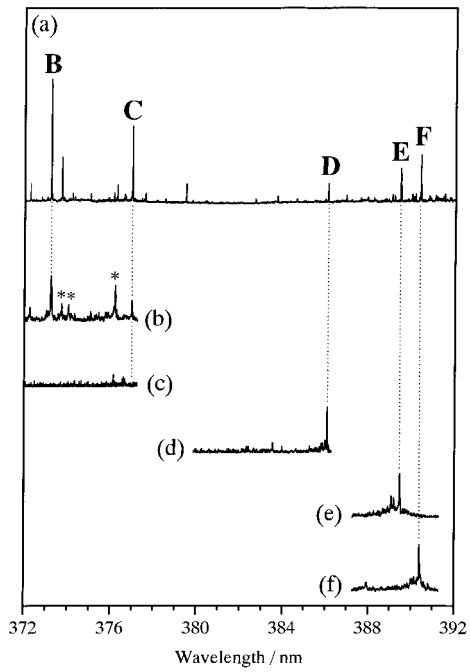

Figure 2. (a) FE spectrum exhibiting the origin bands for species B−F. Two-color resonance-enhanced two-photon ionization (2C-R2PI) spectra in mass channels corresponding to: (b) AD−$(H_2O)_1^+$, (c) AD−$(H_2O)_2^+$, (d) AD−$(H_2O)_3^+$, (e) AD−$(H_2O)_4^+$, and (f) AD−$(H_2O)_5^+$. The correspondences of the observed bands in the FE and 2C-R2PI spectra are shown with dotted lines. Wavelength for the ionization laser (λ_{ion}) was set to 270 nm for (b) and (c), 277 nm for (d), 275 nm for (e) and (f). The bands denoted by asterisks in (b) are due to nonfluorescent hydrated AD cluster(s), which do not appear in the FE spectrum (see paper III for further discussion).

The assignment of the band A to the AD monomer has been confirmed by the FDIR and 2C-R2PI measurements (see the accompanying papers II and III). The extremely weak fluorescence from the $^1(\pi,\pi^*)$ state of the monomer suggests that nonradiative processes are very fast under the isolated condition. On the other hand, these nonradiative processes are drastically suppressed by microscopic hydration, as demonstrated by the much stronger cluster bands appearing in the FE spectrum. Such behaviors in jet-cooled AD and its hydrated clusters are parallel to those of AD in condensed phases,[23,32−34] as described in the Introduction and discussed in detail in paper III.

3.2. Mass Assignments of Hydrated AD Clusters. To determine the number of solvents in relatively smaller clusters, we have performed mass-selective experiments. First, appearances of photoions from species B were observed by scanning λ_{ion} with λ_{res} fixed to its electric origin. The AD^+-H_2O ion came to appear when λ_{ion} went below 280 nm, confirming the species as a 1:1 cluster. Fragmentation into the AD^+ channel was observed with $\lambda_{ion} < 260$ nm, and thus the dissociation energy for $AD^+-H_2O \rightarrow AD^+ + H_2O$ was settled to be ≥ 3000 cm^{-1}. In general, the ionization threshold of the hydrogen-bonded complex does not correspond to the adiabatic ionization potential of the complex, so the true dissociation energy for this system must certainly be larger than this lower limit. Next, 2C-R2PI excitation measurements were conducted with $\lambda_{ion} \approx$ 270 nm for species B and ≈ 275 nm for species C−F. Spectra thus obtained by monitoring the AD$^+$−$(H_2O)_n$ (n = 1−5) channels are presented in Figure 2. As the λ_{ion} photon energy

for species C−F was smaller than the dissociation threshold in AD^+-H_2O by ≈2000 cm^{-1}, fragmentation into lower mass channels does not occur also in the higher clusters except for species C, which is mentioned below. Therefore, species D, E, and F were assigned to the hydrated clusters with $n = 3$, 4, and 5, respectively.

Species C has been observed in the AD^+-H_2O channel, but the fluorescence-detected IR measurement has indicated that this species is an $AD-(H_2O)_2$ cluster, as will be mentioned in paper II. Thus, loss of one water molecule from $AD-(H_2O)_2$ always accompanies photoionization by $\lambda_{ion} = 250-280$ nm, as indicated by the complete absence in the parent $AD^+-(H_2O)_2$ channel (Figure 2c). Such efficient fragmentation has also been reported for indole$-(H_2O)_2$ (ref 43) and the C═O bonded 1:2 hydrated cluster of *N*-phenyl formamide,[44] and attributed to the large conformational changes in the clusters after photoionization. In the case that the stable geometry in the ionic state is so different from that in the neutral S_1 state, the Franck−Condon region for the ion ← S_1 excitation is inevitably located at highly excited vibrational levels in the ionic state, which are well above the dissociation limit into fragments. It is unclear at this moment why only the $n = 2$ cluster causes such severe fragmentation after photoionization.

In the present experiments, no ion signals of bare AD were observed by the threshold (1 + 1′) ionization, i.e., λ_{ion} was set just enough to reach the IE_v. This is due to the extremely rapid nonradiative processes in the singlet manifold of bare AD. We have succeeded in observing the 2C-R2PI spectrum of bare AD by applying delayed ionization via triplet manifold,[45−48] as will be discussed in paper III. It is also noted that several new features, denoted with asterisks in Figure 2b, have been observed in the 2C-R2PI spectrum recorded in the AD^+-H_2O channel. These bands are completely absent in the FE spectrum and may be attributed to different isomer(s) with $n \geq 1$, in which nonradiative processes are as fast as in bare AD. Details will be mentioned in paper III.

Species H has been assigned to a hydrated cluster with $n = 6$ by also recording its 2C-R2PI spectrum in the $AD^+-(H_2O)_6$ channel with $\lambda_{ion} = 275$ nm (not shown). For species L, slight two-photon enhancement was observed in the $AD^+-(H_2O)_9$ channel, indicating that it contains nine waters or more. Further experiments are definitely needed to confirm the size assignments of this species and the other higher clusters (G, I−K, M and N).

4. DFT-Optimized Geometries of Hydrated AD Clusters.

4.1. Hydrated AD Clusters with $n = 1$ and 2. As the AD molecule has multiple H bond interacting sites, i.e., the C═O group, the N−H group, and the π clouds of the aromatic rings, various low-lying minimum-energy structures may exist for the $AD-(H_2O)_n$ clusters. All of the possible optimum geometries have been investigated for $n = 1$ and 2 by the DFT calculations at the B3LYP/6-31G(d,p) level. Here we summarize the structures and the energy ordering of the hydrated AD clusters thus identified in the present work. On the basis of these calculations, the spectral shifts in the electronic transition are evaluated to be compared with the observed values, as described in section 5. Harmonic vibrational frequencies and infrared intensities have also been calculated for those structures and are used to simulate infrared spectra for the clusters, as described in paper II.

$AD-(H_2O)_1$. Geometrical optimization for $n = 1$ has identified two minimum-energy structures, which are indicated as **I** and **II** in Figure 3. Initial configurations with the water molecule put on the AD's aromatic rings have been collapsed into each of the optimized structures. Calculated binding energies at the optimized geometries are listed in Table 2. $AD-(H_2O)_1$ **I** is a "C═O bonded" type: one O−H bond of water is directed to the lone-pair electrons of carbonyl with the O···H−O angle of ≈120°. The dangling ("free") O−H bond is almost perpendicular to the molecular plane of AD. The oxygen atom of H_2O, located approximately in the AD plane, seems to interact weakly with 1-hydrogen of the AD chromophore. In the "N−H bonded" type $AD-(H_2O)_1$ **II**, the oxygen atom of water accepts the N−H site hydrogen and the hydrogen atoms of H_2O are slightly off from the reflection plane for C_s symmetry. The C═O bonded isomer (**I**) is slightly more stable than the N−H bonded form (**II**) at the B3LYP/6-31G(d,p) level without BSSE corrections, but the relative stabilities between them are reversed after corrections.

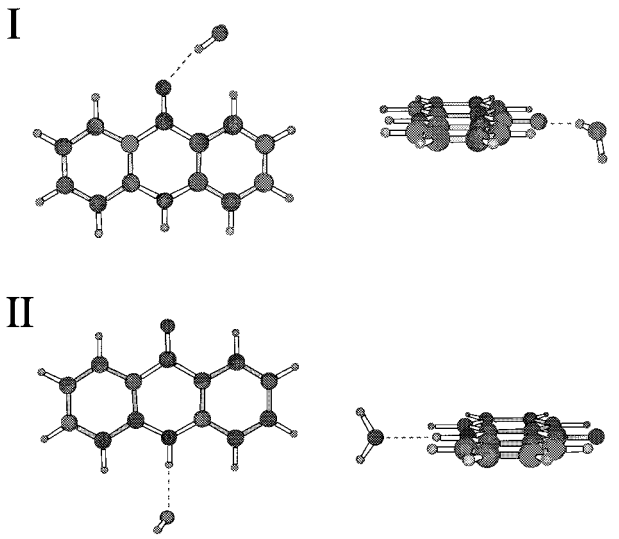

Figure 3. Optimized structures (left: top view, right: side view) for $AD-(H_2O)_1$ at the B3LYP/6-31G(d,p) level. In the top view, the C═O and N−H sites are in the upper and lower halves of the AD molecule, respectively, and C═O points to the right while N−H points to the left in the side view. This orientation of the AD chromophore also holds throughout in Figures 4−7. **I** and **II** are C═O bonded and N−H bonded-type structures, respectively. Possible H bonds are indicated as broken lines.

$AD-(H_2O)_2$. Geometrical optimization for $n = 2$ has yielded four stable structures, which are indicated as **I**−**IV** in Figure 4. Their calculated binding energies are listed in Table 2. $AD-(H_2O)_2$ **I** is a "C═O bonded" type. Its geometry is approximated as the $AD-(H_2O)_1$ **I** cluster bound by another water (denoted #2 in Figure 4), which acts as an H donor to the first water (#1). Both of the oxygen atoms in the waters lie nearly in the AD molecular plane. The structure of the $(H_2O)_2$ unit is a slightly distorted form of the free water dimer.[49] The second isomer, $AD-(H_2O)_2$ **II**, is an "N−H bonded" type, in which the first water (#1) accepts the N−H site hydrogen and the second water (#2) acts in turn as an H acceptor for #1. Water #2, located above the AD molecular plane, interacts with the π cloud of AD's aromatic ring. For making the π-H bond in keeping with the H bonding between the waters, the orientation of the first water is substantially altered from that in $AD-(H_2O)_1$ **II** of the same "N−H bonded" type. The other two isomers, $AD-(H_2O)_2$ **III** and **IV**, correspond to "separately bonded" types, in which both the C═O and N−H sites are H bonded independently by water molecules. Their structures are essentially combinations of the "C═O bonded" [$AD-(H_2O)_1$ **I**] and "N−H bonded" [$AD-(H_2O)_1$ **II**] clusters for $n = 1$. The

TABLE 2: DFT-Calculated Binding Energies, Changes in HOMO and LUMO Orbital Energies, and Spectral Shifts in the Lowest (π,π^*) Transitions of Acridone$-(H_2O)_n$ ($n = 1-5$) at the B3LYP/6-31G(d,p) Level

species	$-\Delta E_e^{N}$ [a] kcal·mol^{-1}	$-\Delta E_0^{N}$ [a] kcal·mol^{-1}	$-\Delta E_0^{B}$ [a] kcal·mol^{-1}	ΔE_{HOMO} [b] cm^{-1}	ΔE_{LUMO} [b] cm^{-1}	$\Delta\nu(\pi,\pi^*)$ [c] cm^{-1}
$n = 1$						
I	9.8	7.6	3.9	−1344	−1865	−521
II	9.0	7.4	4.8	+2860	+2293	−567
$n = 2$						
I	21.1	16.6	9.8	−1511	−2293	−782
II	21.4	17.0	11.1	+1395	+595	−800
III	19.1	15.3	9.2	+1458	+463	−995
IV	19.1	15.3	9.3	+1476	+463	−1013
$n = 3$						
I	33.1	26.4	19.8	+250	−1155	−1405
II	33.2	26.4	17.7	−1502	−2521	−1019
III	34.9	28.1	19.9	+1458	+615	−843
IV	35.0	27.3	15.8	−1676	−2313	−637
V	34.4	27.0	17.0	+1889	+1428	−543
$n = 4$						
I	50.3	40.7	30.6	+242	−1522	−1764
II	46.7	37.8	26.6	+1432	+463	−969
III	51.7	41.3	28.4	+1926	+1428	−498
$n = 5$						
I	64.8	52.9	39.1	−1023	−2963	−1940
II	63.2	51.1	37.4	+281	−1583	−1864
III	64.8	52.2	39.0	+1197	+589	−608

[a] Total binding energy. The superscripts N and B represent without and with BSSE corrections, and the subscripts e and 0 denote without and with ZPVE corrections, respectively. [b] HOMO or LUMO orbital energy relative to that of bare AD. [c] $\Delta\nu(\pi,\pi^*) = \Delta E_{LUMO} - \Delta E_{HOMO}$.

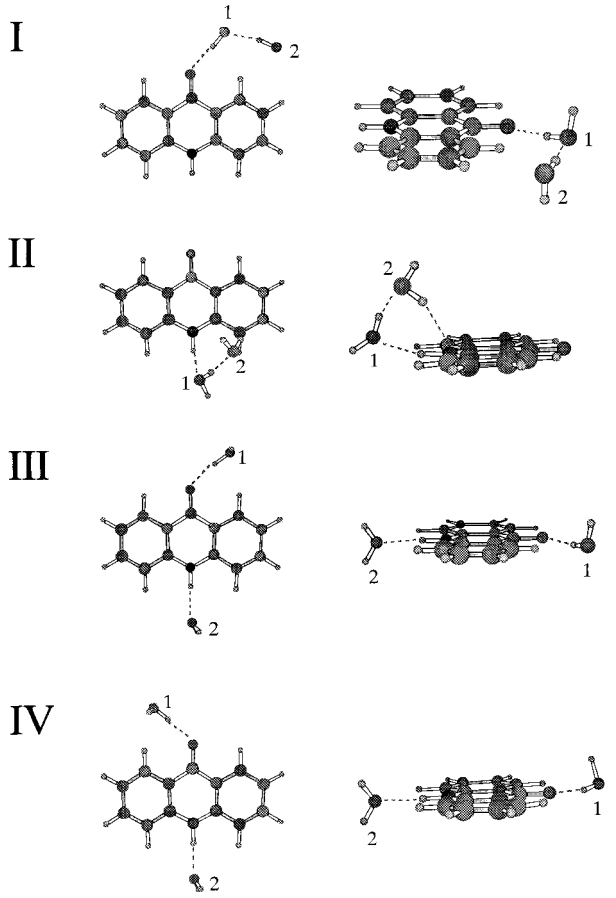

Figure 4. Optimized structures for AD$-(H_2O)_2$ at the B3LYP/6-31G-(d,p) level. **I**: C═O bonded type, **II**: N−H bonded type, **III**: cis separately bonded type, and **IV**: trans separately bonded type. Numbering of each water molecule is given.

only difference between them is the relative orientation of the two waters, which are tilted toward the same direction in AD$-(H_2O)_2$ **III**, i.e., cis configuration, while to the opposite directions (trans) in AD$-(H_2O)_2$ **IV**.

According to the calculated binding energies for the four stable isomers listed in Table 2, the N−H bonded type [AD$-(H_2O)_2$ **II**] is most stable and the C═O bonded type [AD$-(H_2O)_2$ **I**] is the second at the B3LYP/6-31G(d,p) level. The energy difference between them becomes larger after BSSE corrections from 0.4 to 1.3 kcal/mol. The two separately bonded type isomers [AD$-(H_2O)_2$ **III** and **IV**] are essentially isoenergetic. They are less stable (more than 1.3 kcal/mol) than the others without BSSE corrections, while the difference to the isomer **I** is reduced to 0.5−0.6 kcal/mol after BSSE corrections. It is interesting that the binding energies of **III** and **IV** are 0.3−0.6 kcal/mol greater than the sum of those of AD$-(H_2O)_1$ **I** and **II**, indicating cooperative effect of H bonding to two independent bonding sites.

4.2. Hydrated AD Clusters with $n = 3-5$. Since there are many possible isomeric forms at these aggregation levels, it is extremely difficult to carry out a global survey for local minima with $n = 3-5$ as extensively as we have done for the smaller size clusters. Therefore, we have excluded some specific types of minimum-energy structures, which are obtained at the RHF/6-31G level, from the candidates for the B3LYP/6-31G(d,p) optimization as mentioned below.

The binding energies of the separately bonded types, in which $(H_2O)_m$ and $(H_2O)_l$ units ($m, l \geq 1$, $m + l = n$) are independently bound to the C═O and N−H sites of AD, respectively, are much smaller than those of the other types at the RHF/6-31G level. The calculated values for the separately bonded types of $n = 3$ are $\approx$ 3 kcal/mol less than those of the other types, and the energy differences between separately bonded type and the other types become larger with increasing cluster sizes, i.e., $\approx$5 kcal/mol for $n = 4$ and $\approx$10 kcal/mol for $n = 5$. Thus, we did not consider "separately bonded" types in the DFT optimizations for the $n = 3-5$ clusters. Furthermore, as will be described in paper II, the observed FDIR spectra have revealed that H-bond formation between the N−H site and water molecule takes place in the $n \geq 4$ clusters (though it is not so clear in the case of $n = 3$). Therefore, further geometrical optimizations for $n = 4$ and 5 by the B3LYP/6-31G(d,p) calculations were restricted to

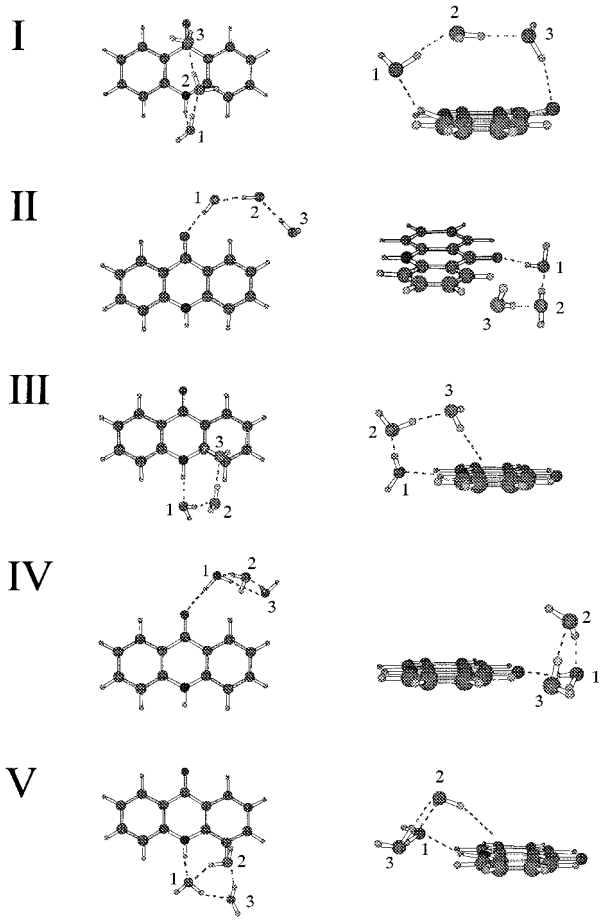

Figure 5. Optimized structures for AD−$(H_2O)_3$ at the B3LYP/6-31G-(d,p) level. **I**: bridged type, **II**: C═O bonded chain type, **III**: N−H bonded chain type, **IV**: C═O bonded cyclic type, and **V**: N−H bonded cyclic type.

the structures involving the N−H···OH_2 H bond, which have been identified at the RHF/6-31G level.

AD−$(H_2O)_3$. For the $n = 3$ cluster, many local minimum-energy structures have been identified by geometry optimization at the RHF/6-31G level, and among them, five structures (except for the separately bonded type) have been further optimized at the B3LYP/6-31G(d,p) level. The stable isomers thus obtained are indicated in Figure 5. They are: one "bridged" type structure (**I**), in which the C═O and N−H sites are bridged by a water chain formed with three solvent molecules, two C═O bonded structures, i.e., "chain" (**II**) and "cyclic" type (**IV**), and two N−H bonded structures, i.e., also "chain" (**III**) and "cyclic" type (**V**). Their calculated binding energies are listed in Table 2.

In the "bridged" isomer **I**, the AD molecule is considerably deformed by the constraint from the water bridge: the C═O and N−H bonds are out of the plane by ≈18° and ≈17°, respectively. In this isomer, the dangling O−H bond of water #2 is nearly parallel to the AD's aromatic rings and prohibited from interacting with the π cloud at the present level of theory. It is noted that water #3 in the bridged isomer (**I**) forms a kind of π-type H bond to the O atom in the C═O group, in contrast to the others (**II** and **IV**) with σ-type H bonds to the lone-pair electrons of carbonyl (see Figure 5). In AD−$(H_2O)_3$ **II**, the AD−$(H_2O)_2$ unit is essentially the same as the $n = 2$ cluster **I**. Another water molecule (#3), whose O atom also lies approximately in the AD molecular plane, further hydrogen-donates to the second one (#2). Consequently, an H-bonded chain of three waters surrounds the edge of the AD molecule

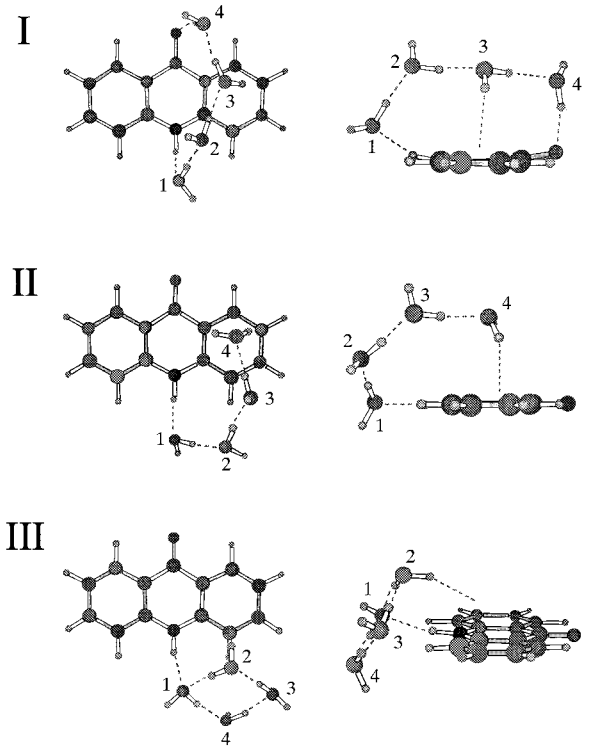

Figure 6. Optimized structures for AD−$(H_2O)_4$ at the B3LYP/6-31G-(d,p) level. **I**: bridged type, **II**: N−H bonded chain type, and **III**: N−H bonded cyclic type.

in the plane of the aromatic rings. AD−$(H_2O)_3$ **III** is of type analogous to AD−$(H_2O)_2$ **II**: the water chain bridges the N−H site and the π cloud of the AD's aromatic ring. Orientation of water #1 becomes much closer to that in AD−$(H_2O)_1$ **II** compared to the $n = 2$ cluster (**II**), probably because of smaller constraint in the longer water chain. In isomers **IV** and **V**, the cyclic $(H_2O)_3$ unit quite close to the free water trimer[50] in geometry is H bonded to the C═O or N−H site, respectively. The $(H_2O)_3$ unit in the C═O bonded cyclic type (**IV**) is almost perpendicular to the AD molecular plane, while it is tilted substantially toward the AD's aromatic rings to form a π-H bond in the N−H bonded cyclic type (**V**).

As listed in Table 2, the N−H bonded chain type (**III**) is most stable among the five conformers for the $n = 3$ clusters at the B3LYP/6-31G(d,p) level. Its binding energy is larger by 0.8−1.7 kcal/mol than the others without BSSE corrections. However, BSSE corrections largely reduce the energy margin between the N−H bonded chain (**III**) and the bridged isomers (**I**), which is only 0.1 kcal/mol. At the present calculation level, it is thereby difficult to conclude that the global minimum energy structure is whether the isomer is **I** or **III**. The other three isomers, **II**, **IV**, and **V**, are more than 2 kcal/mol less stable than the isomer **III** after corrections. It is noted that the cyclic types with the H-bonded C═O (**IV**) and N−H (**V**) sites are, respectively, the first and the second most stable among **I**, **II**, **IV**, and **V** without BSSE corrections, but the ordering in stability is completely reversed after BSSE corrections. Therefore, higher level ab inito and/or DFT calculations with a larger basis set would be needed so as to confirm less stabilities of cyclic isomers.

AD−$(H_2O)_4$. Three stable conformers, in which $(H_2O)_4$ interacts with the N−H site of AD, were obtained by the re-optimizations at the B3LYP/6-31G(d,p) level as shown in Figure 6. Their calculated binding energies are listed in Table 2. AD−$(H_2O)_4$ **I** is a "bridged" type, which is analogous to AD−$(H_2O)_3$

I. Due to the increased number of water molecules bridging the C═O and N−H sites over the AD molecule, the constraint in the water bridge seems to be largely relaxed in comparison with the corresponding $n = 3$ cluster. Therefore, water #3 lying on the AD aromatic rings can interact with the π cloud of AD via one of its O−H bonds. Out-of-planarity for the N−H and C═O bonds (≈6° and ≈9°, respectively) is also much smaller than that in AD−$(H_2O)_3$ **I**. The second isomer AD−$(H_2O)_4$ **II** is an "N−H bonded chain" type analogous to AD−$(H_2O)_2$ **II** and AD−$(H_2O)_3$ **III**, and four water molecules in the cluster bridge between the N−H site and the π cloud of the AD's aromatic ring. The third isomer AD−$(H_2O)_4$ **III** can be classified as an "N−H bonded cyclic" type, which is analogous to AD−$(H_2O)_3$ **V**. Structure of its $(H_2O)_4$ unit is quite similar to that of the free cyclic water tetramer.[51] This water unit is bound to the N−H hydrogen at the O atom of water #1, and slightly tilted toward the AD's aromatic rings to allow the hydrogen of water #2 to interact with the π cloud.

As listed in Table 2, the binding energies for the three isomers **III**, **I**, and **II** are in decreasing order at the B3LYP/6-31G(d,p) level without BSSE corrections, but the bridged form (**I**) becomes more stable than the N−H bonded cyclic form (**III**) by 2.2 kcal/mol after BSSE corrections. The definitive conclusion on the relative stability for the isomer **I** and **III** thereby should await calculations with larger basis set including diffuse functions. The "N−H bonded chain" type isomer **II** is less stable than the other two types, in contrast to the $n = 2$ and 3 cases, for which the cluster of this type corresponds to the global minimum. This is simply explained by numbers of the possible H bonds in these structural isomers. In AD−$(H_2O)_4$ **II**, there are five H bonds, of which four are σ-type and the other is π-type, whereas both AD−$(H_2O)_4$ **I** and **III** have another H bond between water and the C═O site (**I**) or two waters (**III**).

AD−$(H_2O)_5$. Four N−H bonded stable structures identified at the RHF/6-31G level were further optimized by the DFT calculations. One of the isomeric forms, i.e., "N−H bonded chain" type analogous to AD−$(H_2O)_4$ **II**, has been found unstable at the B3LYP/6-31G(d,p) level. The resultant three minimum-energy structures are indicated in Figure 7. They are divided into two types: AD−$(H_2O)_5$ **I** and **II** are "bridged" types and AD−$(H_2O)_5$ **III** is an "N−H bonded cyclic" type. In the bridged type isomers **I** and **II**, constraint in a water bridge seems to be further relaxed in comparison with their smaller-size analogues, i.e., AD−$(H_2O)_3$ **I** and AD−$(H_2O)_4$ **I**, as indicated by the almost planar AD molecule in the $n = 5$ clusters. Five water molecules are sufficient to form a flexible bridge between the C═O and N−H sites of AD, and, as a result, two different bridge conformations are allowed as in **I** and **II**. In AD−$(H_2O)_5$ **I**, there are eight H bonds in total: five σ-type among waters and the N−H site, one π-type between water #5 and the C═O oxygen of AD, and two π-H-bonding interactions between waters (#3 and #4) and the AD aromatic rings. The σ-H-bonded O−H of waters #2−#4 lie approximately in a plane parallel to the AD aromatic rings (see the side view of **I** in Figure 7). In AD−$(H_2O)_5$ **II**, the free O−H bond of water #3 nearly points to the opposite direction to that in isomer **I**, hence there is only one π-H bond interacting with the aromatic ring, whereas the H bonds of the σ-type and the C═O bound π-type are the same as **I**. This deformation causes rather irregular directions of the σ-H bonds in the water bridge. The third isomer AD−$(H_2O)_5$ **III** is analogous to AD−$(H_2O)_3$ **V** and AD−$(H_2O)_4$ **III**. The $(H_2O)_5$ unit, which resembles the free cyclic water pentamer,[52] is bound to the N−H hydrogen in the cluster. The water pentamer is tilted to form two π-H bonds between water molecules (#2 and #4) and the AD aromatic rings.

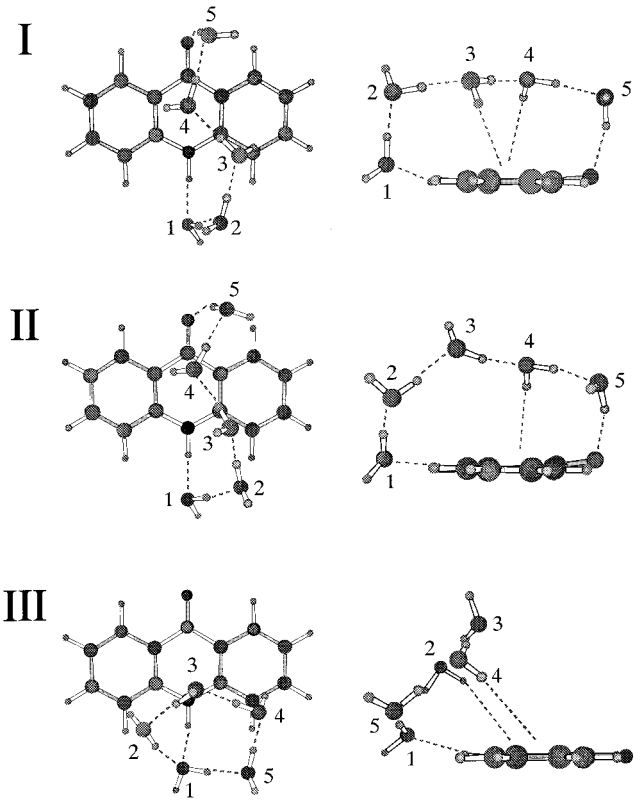

Figure 7. Optimized structures for AD−$(H_2O)_5$ at the B3LYP/6-31G(d,p) level. **I**: bridged type, **II**: bridged type, and **III**: N−H bonded cyclic type.

The conformational variation in the water bridge mentioned above causes a difference in stability for the two bridged isomers: the BSSE-corrected binding energy of AD−$(H_2O)_5$ **I** is 1.7 kcal/mol greater than that of AD−$(H_2O)_5$ **II** at the B3LYP/6-31G(d,p) level. The isomer **I** is slightly more stable than **III**, but the difference (0.1 kcal/mol) is marginal at this level of theory. The higher level ab initio or DFT calculations must be performed for more accurate prediction of the relative stability between **I** and **III**.

5. Characterization of Solvent Geometry via Spectral Shifts

Spectral shifts in the electronic transition are caused by modification of the electronic wave functions of both the upper and lower states by cluster formation. The shifts are sensitive to geometrical configuration of the clusters, especially for species with relatively strong intermolecular interactions, e.g., hydrogen bonding, and thus may be used as a useful experimental source for structural characterization of clusters. Here, we adopt a method for estimating spectral shifts by utilizing molecular-orbital calculations, which has been applied by Kleinermanns and co-workers.[53] The method is based on an extremely rough approximation which assumes the $S_1 \leftarrow S_0$ transition as an one-electron excitation from the HOMO (highest occupied molecular orbital) to the LUMO (lowest unoccupied molecular orbital). The MOs are further approximated to be unchanged regardless of the electronic excitations. This frozen-orbital approximation enables us to estimate the HOMO−LUMO excitation energy once the ground-state orbitals are evaluated. Of course, this approach is oversimplified to reproduce the absolute values of the transition energies, but relative

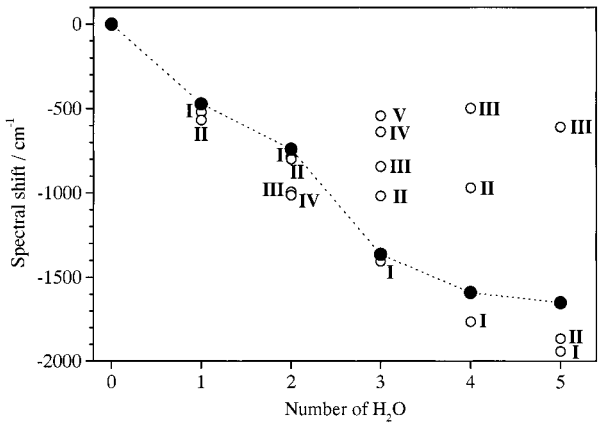

Figure 8. Spectral shifts in the $^1(\pi,\pi^*)$ transition of AD$-(H_2O)_n$ ($n = 1-5$) plotted against the number of water molecules. Closed and open circles denote the observed and calculated values, respectively, and roman numbers (**I**, **II**, ...) correspond to the optimized structures shown in Figures 4−7.

spectral shifts by stepwise hydration can be quantitatively reproduced. It has been exemplified by the results on the hydrated *p*-cresol clusters with $n = 1-3$, of which the HOMO−LUMO excitation has been evaluated with the Hartree−Fock (HF) calculations with minimal basis sets.[53]

In the present study, the HOMO−LUMO excitation energies have been calculated by DFT for the minimum-energy conformers of the hydrated AD clusters with $n = 1-5$ at the B3LYP/6-31G(d,p) level. Comparisons of the experimental shifts in the $^1(\pi,\pi^*)$ transition with the calculated ones have been performed to estimate the geometry of the observed clusters. Such a utility is given in full play by correlating the analyses of the FDIR spectra, which will be described in paper II. It is noted that the use of DFT one-electron energy differences to estimate excitation energies is often a matter of debate.[54−62] In contrast to the HF theory, in which one-electron orbitals are used to minimize the energy directly, Kohn−Sham (KS) orbitals in DFT are used to construct the correct electron density. The energies of the KS orbitals, therefore, do not provide a simple physical meaning as the HF orbitals do.[54] However, DFT calculations on the excitation energy via HOMO−LUMO energy differences have been performed for several conjugated π systems, and it has been proved that the HOMO−LUMO energy differences with DFT calculations yield excitation energies in good agreement with experimental values.[63,64]

Figure 8 shows the plot of the observed and calculated spectral shifts of the $n = 1-5$ clusters as a function of the solvent numbers. The electron distributions in the HOMO and LUMO orbitals for bare AD are schematically shown in Figure 9. In the HOMO (the highest π orbital), the charge distribution is mainly localized on the N−H group, while in the LUMO (the lowest π^* orbital), the electron density is substantially large at the C═O group. Therefore, the lowest $\pi^* \leftarrow \pi$ transition of the AD molecule is of intramolecular charge-transfer type from the N−H group to the C═O group.[35,42] The drastic change of the charge distribution in the HOMO and LUMO provides the spectral shifts characteristic to the solvent numbers and the cluster conformations as follows.

AD−(H$_2$O)$_1$. When the C═O group is bound by the H_2O molecule which acts as the proton donor (isomer **I** in Figure 3), both the HOMO and LUMO are largely stabilized, as listed in Table 2. The stabilization energy is larger for the LUMO (π^* orbital) than the HOMO (π orbital) because of the larger electron density at the C═O group in the LUMO. Therefore, the $\pi^* \leftarrow \pi$ transition of the C═O bonded isomer **I** shows a

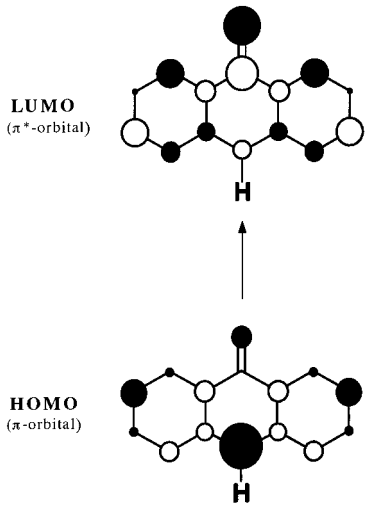

Figure 9. Schematic representation of the HOMO and LUMO of the AD molecule. Size of the circles represents the coefficient of pπ-atomic orbitals in the MO, with indicating the relative phases as open or closed circles.

red shift. When the N−H group is bound by water which acts as proton acceptor (isomer **II** in Figure 3), both the HOMO and LUMO are largely destabilized in contrast to the C═O bonded isomer **I**, and the destabilization of the HOMO is larger than the LUMO. This is due to the higher acidity of the N−H group in the HOMO than in the LUMO. Therefore, the $\pi^* \leftarrow \pi$ transition of the N−H bonded isomer **II** also shows a red shift. The calculated spectral shifts are almost the same in isomers **I** and **II**: -521 cm^{-1} in **I** (C═O bonded) and -567 cm^{-1} in **II** (N−H bonded). Both of them are in reasonable agreement with the experimental value (-472 cm^{-1}) for the $n = 1$ cluster (species B), though the quantitative correspondence between the observed and calculated shifts is better in isomer **I**. Thus it is difficult to clarify the geometry of the species B only from the discussion on the spectral shifts, and the results of the FDIR spectrum should be invoked.

AD−(H$_2$O)$_2$. The calculations predict that the lowest $\pi^* \leftarrow \pi$ transition in all of the four minimum-energy structures (**I**−**IV**) of the $n = 2$ clusters show red shifts. In the C═O bonded isomer **I**, both the stabilization energies of the HOMO and LUMO are larger than in the AD$-(H_2O)_1$ **I**, especially for the LUMO. As a result, AD$-(H_2O)_2$ **I** is estimated to be further red-shifted from AD$-(H_2O)_1$ **I** by 261 cm^{-1}. In the N−H bonded isomer **II**, the red shift is also increased from the N−H bonded $n = 1$ cluster (**II**) and is almost the same with that in the C═O bonded isomer **I**. It is noted that the destabilization of the HOMO and LUMO in isomer **II** is much smaller than that in AD$-(H_2O)_1$ **II**. This might be due to the interaction between the π-cloud of AD and water #2 in AD$-(H_2O)_2$ **II**. The calculated spectral red shifts of both of the separately bonded isomers (**III** and **IV**) are about 1000 cm^{-1}. These clusters are essentially additions of the "C═O bonded" [AD$-(H_2O)_1$ **I**] and "N−H bonded" [AD$-(H_2O)_1$ **II**] clusters for $n = 1$, as mentioned before. This is evidently reflected in the HOMO and LUMO enegetics of the separately bonded isomers: ΔE_{HOMO} and ΔE_{LUMO} of these isomers are nearly equal to the sum of ΔE_{HOMO} and ΔE_{LUMO} of AD$-(H_2O)_1$ **I** and **II**, respectively, resulting in additivity in their calculated spectral shifts (see Table 2).

As listed in Table 2, the situation in the match-up between the observed and calculated spectral shifts is similar to that in the $n = 1$ cluster. Both the C═O bonded (**I**) and N−H bonded (**II**) isomers show the calculated shifts which are in good

agreement with the observed value, and thus we have to await the FDIR measurements for structural determination of the species C ($n = 2$). On the other hand, the shifts in the separately bonded isomers (**III** and **IV**) are too large as compared with the observed value. This excludes the possibility for assignment of species C as the separately bonded isomers, and is consistent with their calculated stabilities which are inferior to the isomers **I** and **II**.

AD−(H$_2$O)$_3$. HOMO−LUMO gap calculation for the five stable conformers of the $n = 3$ clusters reveals that the magnitudes of the shifts are quite different from each other, as listed in Table 2. The bridged-type isomer **I** in which three water molecules bridge between the C═O and N−H sites on the AD chromophore shows the largest red shift (1405 cm^{-1}) among the five conformers, which reproduces quite well the observed large red shift of 1364 cm^{-1} in species D ($n = 3$). On the other hand, the shifts in all the other conformers are too small compared with the observed value. This result indicates that the observed $n = 3$ cluster should be of the bridged-type geometry. It is noted that the HOMO is destabilized while the LUMO is largely stabilized in case of the bridged-type conformer, since the C═O and N−H sites are both H bonded in this isomer. This results in the substantially large red shift in this conformation (see Table 2).

The chain-type isomers **II** and **III** of $n = 3$ show further red shifts from the smaller analogues, i.e., AD−(H$_2$O)$_2$ **I** and **II**, but their increments become smaller than those by the association with the first and second waters: 521 (first) → 261 (second) → 237 cm^{-1} (third) in the C═O bonded isomers, and 567 (first) → 233 (second) → 43 cm^{-1} (third) in the N−H bonded isomers. In the cyclic-type isomers **IV** and **V** of $n = 3$, the spectral red shifts are much smaller than those in the bridged and chain types.

AD−(H$_2$O)$_4$. The magnitudes of the calculated spectral shifts of the three candidates for species E ($n = 4$), i.e., the bridged-type isomer **I**, the N−H bonded chain-type isomer **II**, and the N−H bonded cyclic isomer **III**, are also quite different from one another. The bridged form of the $n = 4$ cluster shows much larger red shift than the other two isomers as listed in Table 2. This is due to the same reason as the bridged-type isomer for $n = 3$: the HOMO is slightly destabilized while the LUMO is largely stabilized to decrease the HOMO−LUMO energy gap. Therefore, only the bridged isomer **I** reproduces the large red shift (1589 cm^{-1}) for the observed species E, and the other two isomers never do. This result indicates that the observed $n = 4$ cluster should be of the bridged-type geometry as in the case of $n = 3$. It is noted that agreement between the observed and calculated shifts becomes worse for $n = 4$. This may be due to inaccuracy in calculation level adopted in the present study to describe the interaction between the π-cloud of AD and waters, which would make more contribution to stabilize the HOMO in the bridged-type cluster.

AD−(H$_2$O)$_5$. Among the three stable isomers of $n = 5$, the bridged-type isomers **I** and **II** show large red shifts, whereas the N−H bonded-type isomer **III** shows a relatively small red shift. The difference in the spectral shifts between the bridged and N−H bonded cyclic types is more than 1200 cm^{-1}. Though the calculated spectral shifts in the bridged types are somewhat larger than the experimental shift of species F ($n = 5$), the values for the bridged isomers **I** and **II** are much closer to the experimental observation than that for the N−H bonded isomer **III**. Therefore, the observed $n = 5$ cluster should be the bridged-type isomer **I** or **II**, as for the $n = 3$ and 4 clusters. The conformer **I** is most probable as species F judging from the calculated relative stabilities (see Table 2). It is noted that both the HOMO and LUMO in the bridged-type conformer are stabilized largely in the case of $n = 5$. This may be correlated to the larger flexibility in the water bridge in the $n = 5$ cluster, which allows the water molecules to interact more effectively with the π cloud of the AD chromophore.

6. Conclusions

As the first part of investigation on structure and dynamics of AD and its hydrated clusters, the electronic transitions associated with the lowest $^1(\pi,\pi^*)$ excitation have been reported in the present paper. Many vibronic bands, identified in the 370−400 nm region by the FE measurements, have been attributed to 14 different species, i.e., the AD monomer and 13 fluorescent hydrated clusters, by UV−UV hole-burning spectroscopy. Mass-selective 2C-R2PI experiments have provided definitive size assignments for relatively smaller clusters, AD−(H$_2$O)$_n$ ($n = 1-6$). The origin bands of all the hydrated clusters are red shifted, and the shifts increase as the cluster sizes become larger and are approaching to the value in bulk solution. However, their changes are not monotonic: the incremental shift is reduced to almost half from $n = 1$ to 2 but becomes largest for $n = 3$, followed by much smaller increments for $n \geq 4$.

To explore possible minimum-energy structures for $n = 1-5$ and to explain the above-mentioned spectral shifts in the $^1(\pi,\pi^*)$ transition, DFT calculations have been conducted at the B3LYP/6-31G(d,p) level. For smaller-size clusters of $n = 1$ and 2, two geometrical isomers with almost identical stability have been identified, i.e., the N−H bonded and C═O bonded forms. The calculated HOMO−LUMO gaps in the two isomers are both in good agreement with the observed spectral shifts, and thus more experimental information from, for example, FDIR spectroscopy has to be invoked for definitive structural assignments. For the $n = 3$ cluster, five minimum-energy structures have been identified within 4 kcal/mol in binding energy. Comparison between the observed and calculated spectral shifts strongly suggests that the observed species of this size should be assigned to the bridged form with the N−H and C═O sites of AD bound by a water chain, despite that this conformer is calculated to be slightly less stable than the N−H bonded chain type form. The bridged forms become the most stable forms for the larger-size clusters ($n = 4$ and 5), even though other isomeric forms are located quite close in binding energy. As in the case of $n = 3$, the calculated spectral shifts only for the bridged form well reproduce the observed ones.

The monomer band in the FE spectrum is extremely weak, implying substantially small fluorescence quantum yield under isolated conditions. On the other hand, all of the cluster bands are much stronger, and hence the quantum yield seems to be drastically increased by microscopic hydration at relatively earlier aggregation level. In addition, 2C-R2PI has identified another species which does not appear in the FE spectrum and thus should be almost nonfluorescent as bare AD. Nonradiative dynamics in AD and its hydrated clusters will be fully discussed in accompanying paper III, especially in relation to their solvation structure and the change in electronic energy levels.

Acknowledgment. The present work has been supported by Grants-in-Aid (Nos. 08454177, and 10440172) from the Ministry of Education, Science, Culture, and Sports of Japan. Y.O. thanks the financial support from the Japan Securities Scholarship Foundation and the Mitsubishi Chemical Foundation.

References and Notes

(1) Reichardt, C. *Solvents and Solvation Effects in Organic Chemistry*, 2nd ed.; VCH: Weinheim, 1988.

(2) Suppan, P.; Ghoneim, N. *Solvatochromism*; The Royal Society of Chemistry: Cambridge, 1997.
(3) (a) Steadman, J.; Syage, J. A. *J. Chem. Phys*. **1990**, *92*, 4630. (b) Syage, J. A.; Steadman, J. *J. Chem. Phys*. **1991**, *95*, 2497. (c) Steadman, J.; Syage, J. A. *J. Am. Chem. Soc.* **1991**, *113*, 6786. (d) Steadman, J.; Syage, J. A. *J. Phys. Chem.* **1991**, *95*, 10326. (e) Syage, J. A.; Steadman, J. *J. Phys. Chem.* **1992**, *96*, 9606.
(4) (a) Solgadi, D.; Jouvet, C.; Tramer, A. *J. Phys. Chem.* **1988**, *92*, 3313. (b) Jouvet, C.; Lardeux-Dedonder, C.; Richard-Viard, M.; Solgadi, D.; Tramer, A. *J. Phys. Chem.* **1990**, *94*, 5041.
(5) Heneman, M.; Kelley, D. F.; Bernstein, E. R. *J. Chem. Phys*. **1993**, *99*, 4533.
(6) Cheshnovsky, O.; Leutwyler, S. *J. Chem. Phys*. **1988**, *88*, 4127.
(7) (a) Breen, J. J.; Peng, L. W.; Willberg, D. M.; Heikal, A.; Cong, P.; Zewail, A. H. *J. Chem. Phys*. **1990**, *92*, 805. (b) Kim, S. K.; Breen, J. J.; Willberg, D. M.; Peng, L. W.; Heikal, A.; Syage, J. A.; Zewail, A. H. *J. Phys. Chem.* **1995**, *99*, 7421.
(8) (a) Kim, S. K.; Bernstein, E. R. *J. Phys. Chem.* **1990**, *94*, 3531. (b) Kim, S. K.; Li. S.; Bernstein, E. R. *J. Chem. Phys.* **1991**, *95*, 3119.
(9) (a) Saigusa, H.; Sheng, S.; Lim, E. C. *J. Phys. Chem.* **1992**, *96*, 2083. (b) Saigusa, H.; Sheng, S.; Lim, E. C. *J. Chem. Phys.* **1992**, *97*, 9072. (c) Saigusa, H.; Lim, E. C. *J. Chem. Phys.* **1995**, *103*, 8793. (d) Saigusa, H.; Lim, E. C. *J. Phys. Chem.* **1995**, *99*, 15738.
(10) (a) Honma, K.; Arita, K.; Yamasaki, K.; Kajimoto, O. *J. Chem. Phys.* **1991**, *94*, 3496. (b) Honma, K.; Kajimoto, O. *J. Chem. Phys.* **1994**, *101*, 1752.
(11) Peyor, B. A.; Palmer P. M.; Andrews, P. M.; Berger, M. B.; Topp, M. R. *J. Phys. Chem.* **1998**, *102*, 3284.
(12) (a) Felker, P. M.; Zewail, A. H. *Chem. Phys. Lett.* **1983**, *94*, 448. (b) Felker, P. M.; Zewail, A. H. *Chem. Phys. Lett.* **1983**, *94*, 454.
(13) Zwier, T. S. *Annu. Rev. Phys. Chem.* **1996**, *47*, 205.
(14) Felker, P. M.; Maxton, P. M.; Schaeffer, M. W. *Chem. Rev*. **1994**, *94*, 1787.
(15) Pribble, R. N.; Zwier, T. S. *Science* **1994**, *265*, 75.
(16) Gruenloh, C. J.; Carney, J. R.; Arrington, C. A.; Zweir, T. S. Ferdericks, S. Y.; Jordan, K. D. *Science* **1997**, *276*, 1678.
(17) Watanabe, T.; Ebata, T.; Tanabe, S.; Mikami, N. *J. Chem. Phys*. **1996**, *105*, 408.
(18) Janzen, C.; Spangenberg, D.; Roth, W.; Kleinermanns, K. *J. Chem. Phys*. **1999**, *110*, 9898.
(19) Turro, N. *Modern molecular photochemistry*; Benjamin-Cummings: Menlo Park, CA, 1978.
(20) Amirav, A.; Horwitz, C.; Jortner, J. *J. Chem. Phys*. **1988**, *88*, 3092.
(21) Lim, E. C. *J. Chem. Phys*. **1986**, *90*, 6770.
(22) El-Sayed, M. A.; Kasha, M. *Spectrochim. Acta* **1959**, *15*, 758.
(23) Siegmund, M.; Bendig, J. *Ber. Bunsen-Ges. Phys. Chem*. **1978**, *82*, 1061.
(24) Dalton, J. C.; Montgomery, F. C. *J. Am. Chem. Soc.* **1974**, *96*, 6230.
(25) Kellmann, A. *J. Phys. Chem*. **1977**, *81*, 1195.
(26) Hadley, S. G. *J. Phys. Chem*. **1971**, *75*, 2083.
(27) Kasama, K.; Kikuchi, K.; Yamamoto, S.; Uji-ie, K.; Nishida, Y.; Kokubun, H. *J. Phys. Chem*. **1981**, *85*, 1291.
(28) Struve, W. S.; Hedstrom, J. H.; Morgante, C. G. *J. Chem. Phys*. **1983**, *78*, 7006.
(29) Wassam, W. A.; Lim, E. C. *J. Chem. Phys*. **1978**, *68*, 433.
(30) Mitsui, M.; Ohshima, Y.; Ishiuchi, S.; Sakai, M.; Fujii, M. *Chem. Phys. Lett.* **2000**, *317*, 211.
(31) Mitsui, M.; Ohshima, Y.; Kajimoto, O., to be published.
(32) Kokubun, H.; Kobayashi, M. *Z. Phys. Chem. Neue Folge*. **1964**, *41*, 245.
(33) Fushimi, K.; Kikuchi, K.; Kokubun, H. *J. Photochem.* **1976**, *5*, 457.
(34) Kokubun, H. *Z. Phys. Chem. Neue Folge.* **1976**, *101*, 137.
(35) Inoue, H.; Hoshi, T.; Yoshino, J. *Bull. Chem. Soc. Jpn.* **1972**, *45*, 2653.
(36) Wiley, W. C.; McLaren, I. H. *Rev. Sci. Instrum.* **1955**, *26*, 1150.
(37) Ishijima, S.; Higashi, M.; Yamaguchi, H.; Kubota, M.; Kobayashi, T. *J. Electron. Spectrosc. Relat. Phenom*. **1996**, *82*, 71.
(38) Frisch, M. J.; Trucks, G. W.; Schlegel, H. B.; Scuseria, G. E.; Robb, M. A.; Cheeseman, J. R.; Zakrzewski, V. G.; Montgomery, J. A.; Stratmann, R. E., Jr.; Burant, J. C.; Dapprich, S.; Millam, J. M.; Daniels, A. D.; Kudin, K. N.; Strain, M. C.; Farkas, O.; Tomasi, J.; Barone, V.; Cossi, M.; Cammi, R.; Mennucci, B.; Pomelli, C.; Adamo, C.; Clifford, S.; Ochterski, J.; Petersson, G. A.; Ayala, P. Y.; Cui, Q.; Morokuma, K.; Malick, D. K.; Rabuck, A. D.; Raghavachari, K.; Foresman, J. B.; Cioslowski, J.; Ortiz, J. V.; Stefanov, B. B.; Liu, G.; Liashenko, A. Piskorz, P.; Komaromi, I.; Gomperts, R.; Martin, R. L.; Fox, D. J.; Keith, T.; Al-Laham, M. A.; Peng, C. Y.; Nanayakkara, A.; Gonzalez, C.; Challacombe, M.; Gill, P. M. W.; Johnson, B.; Chen, W.; Wong, M. W.; Andres, J. L.; Gonzalez, C.; Head-Gordon, M.; Replogle, E. S.; Pople, J. A. Gaussian 98; Gaussian, Inc.: Pittsburgh, PA, 1998.
(39) Lee, C.; Yang, W.; Parr, R. G. *Phys. Rev. B* **1988**, *37*, 785.
(40) Becke, A. D. *J. Chem. Phys.* **1993**, *98*, 5648.
(41) Boys, S. F.; Bernardi, F. *Mol. Phys.* **1970**, *19*, 553.
(42) Val'kova, G. A.; Shcherbo, S. N.; Shigorin, D. N. *Docl. Acad. Nauk USSR* **1978**, *240*, 491.
(43) Carney, J. R.; Fredrick, C. H.; Zwier, T. S. *J. Chem. Phys*. **1998**, *108*, 3379.
(44) Dickinson, J. A.; Hockridge, M. R.; Robertson, E. G.; Simons, J. P. *J. Phys. Chem. A* **1999**, *103*, 6938.
(45) Duncan, M. A.; Dietz, T. G.; Liverman, M. G.; Smalley, R. E. *J. Phys. Chem*. **1981**, *85*, 7.
(46) Hiraya, A.; Achiba, Y.; Kimura, K. *J. Chem. Phys*. **1984**, *81*, 3345.
(47) Meijer, G.; Vries, M. S.; Hunziker, H. E.; Wendt, H. R. *J. Phys. Chem*. **1990**, *94*, 4394.
(48) Lipert, R. J.; Colson, S. D. *J. Phys. Chem*. **1990**, *94*, 2358.
(49) Dyke. T. R.; Mack, K. M.; Muenter, J. S. *J. Chem. Phys*. **1977**, *66*, 498.
(50) Pugliano, N.; Saykally, R. J. *Science* **1992**, *257*, 1937.
(51) Cruzan, J. D.; Braly, L. B.; Liu, K.; Brown, M. G.; Loeser, J. G.; Saykally, R. J. *Science* **1996**, *271*, 59.
(52) Liu, K.; Brown, M. G.; Cruzan, J. D.; Saykally, R. J. *Science* **1996**, *271*, 62.
(53) Pohl, M.; Schmitt, M.; Kleinermanns, K. *J. Chem. Phys.* **1991**, *94*, 1717.
(54) Callaway, J.; March, N. H. *Solid State Phys.* **1984**, *38*, 135.
(55) Dreizler, D. M.; Gross, E. K. U. *Density Functional Theory*; Springer: Berlin, 1990.
(56) Godby, R. W.; Schluter, M.; Sham, L. J. *Phys. Rev. B* **1988**, *37*, 10159.
(57) Fritsche, L. *Physica B* **1991**, *172*, 7.
(58) Perdew, J. P.; Levy, M. *Phys. Rev. Lett.* **1983**, *51*, 1884.
(59) Gross, E. K. U.; Oliveira, L. N.; Kohn, W. *Phys. Rev. A* **1988**, *37*, 2805.
(60) Gross, E. K. U.; Oliveira, L. N.; Kohn, W. *Phys. Rev. A* **1988**, *37*, 2809.
(61) Oliveira, L. N.; Gross, E. K. U.; Kohn, W. *Phys. Rev. A* **1988**, *37*, 2821.
(62) Parr, P. G.; Yang, W. *Density-Functional Theory of Atoms and Molecules*; Oxford University Press: New York, 1989.
(63) Salzner, U.; Lagowski, J. B.; Pickup, P. G.; Poirier, R. A. *J. Comput. Chem*. **1997**, *18*, 1943.
(64) Wang, Z.; Day, P. N.; Pachter, R. *J. Chem. Phys*. **1998**, *108*, 2504.